THE JOURNAL OF PHYSICAL CHEMISTRY Letters

Letter

pubs.acs.org/JPCL

Single-Molecule Surface-Enhanced Raman Scattering: Can STEM/EELS Image Electromagnetic Hot Spots?

Nasrin Mirsaleh-Kohan,[†,#] Vighter Iberi,[†,#] Philip D. Simmons, Jr.,[†] Nicholas W. Bigelow,[‡] Alex Vaschillo,[‡] Meng M. Rowland,[†] Michael D. Best,[†] Stephen J. Pennycook,[§,∥] David J. Masiello,*[,‡] Beth S. Guiton,*[,§,⊥] and Jon P. Camden*[,†]

[†]Department of Chemistry, University of Tennessee, Knoxville, Tennessee 37996, United States

[‡]Department of Chemistry, University of Washington, Seattle, Washington 98195, United States

[§]Materials Science and Technology Division, Oak Ridge National Laboratory, Oak Ridge, Tennessee 37831, United States

[∥]Department of Materials Science and Engineering, University of Tennessee, Knoxville, Tennessee 37996, United States

[⊥]Department of Chemistry, University of Kentucky, Lexington, Kentucky 40506, United States

Supporting Information

ABSTRACT: Since the observation of single-molecule surface-enhanced Raman scattering (SMSERS) in 1997, questions regarding the nature of the electromagnetic hot spots responsible for such observations still persist. For the first time, we employ electron-energy-loss spectroscopy (EELS) in a scanning transmission electron microscope (STEM) to obtain maps of the localized surface plasmon modes of SMSERS-active nanostructures, which are resolved in both space and energy. Single-molecule character is confirmed by the bianalyte approach using two isotopologues of Rhodamine 6G. Surprisingly, the STEM/EELS plasmon maps do not show any direct signature of an electromagnetic hot spot in the gaps between the nanoparticles. The origins of this observation are explored using a fully three-dimensional electrodynamics simulation of both the electron-energy-loss probability and the near-electric field enhancements. The calculations suggest that electron beam excitation of the hot spot is possible, but only when the electron beam is located outside of the junction region.

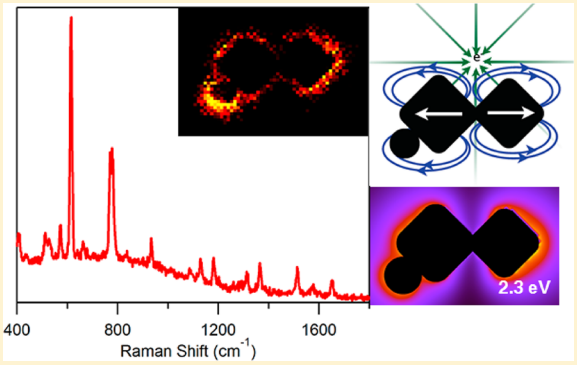

SECTION: Plasmonics, Optical Materials, and Hard Matter

Surface-enhanced Raman scattering (SERS),[1−3] discovered more than three decades ago, relies on the localized surface plasmon resonance (LSPR)[4,5] to deliver large Raman enhancement factors (10^6−10^{10}) to molecules located close to the surface of plasmonic nanostructures. The SERS effect is so dramatic that, despite the weakness of Raman scattering, the vibrational spectrum of a single molecule can be easily observed.[6,7] The claims of single-molecule SERS (SMSERS) were initially met with skepticism because of the extraordinary enhancements proposed (~10^{15}), and efforts immediately turned to proving the existence of SMSERS[8−10] and characterizing the nanostructures that gave rise to such massive enhancements.[11−14] More than 15 years later it has become widely accepted that electromagnetic hot spots play a major role in SMSERS. In the electromagnetic mechanism (EM) of SERS, excitation of the LSPR in a plasmonic nanostructured material leads to a significant electric field enhancement (EFE) at the particle surface, and the Raman cross section of molecules in this enhanced field can be increased by several orders of magnitude.[5,15] Electromagnetic enhancements of 10^{10}−10^{11} at the junction between two closely spaced metallic particles (hot spots) have been predicted,[11,16,17] although the maximum achievable enhancements are moderately reduced when quantum effects are taken into account.[18] Also, studies have shown that more modest enhancement factors (on the order of 10^7−10^8) are sufficient to observe a single molecule in SERS for a resonant molecule such as Rhodamine 6G (R6G).[19]

While the idea of electromagnetic hot spots in SERS is well-known,[20,21] Brus and co-workers[22,23] showed using polarization studies that hot spots formed at the junction of two nanoparticles likely play a major role in SMSERS. This claim was further supported by atomic force microscopy showing that SMSERS-active structures are aggregates of Ag nanoparticles. A study correlating high-resolution transmission electron microscopy (HRTEM), SMSERS, and LSPR showed that multiple aggregate nanostructures ~100 nm in size were suitable for observing SMSERS and continuum electrodynamics calculations on the simplest SMSERS-active aggregates, also confirming that the hot spot was located near the interparticle

Received: July 16, 2012
Accepted: August 3, 2012
Published: August 3, 2012

   dx.doi.org/10.1021/jz300967q | J. Phys. Chem. Lett. 2012, 3, 2303−2309

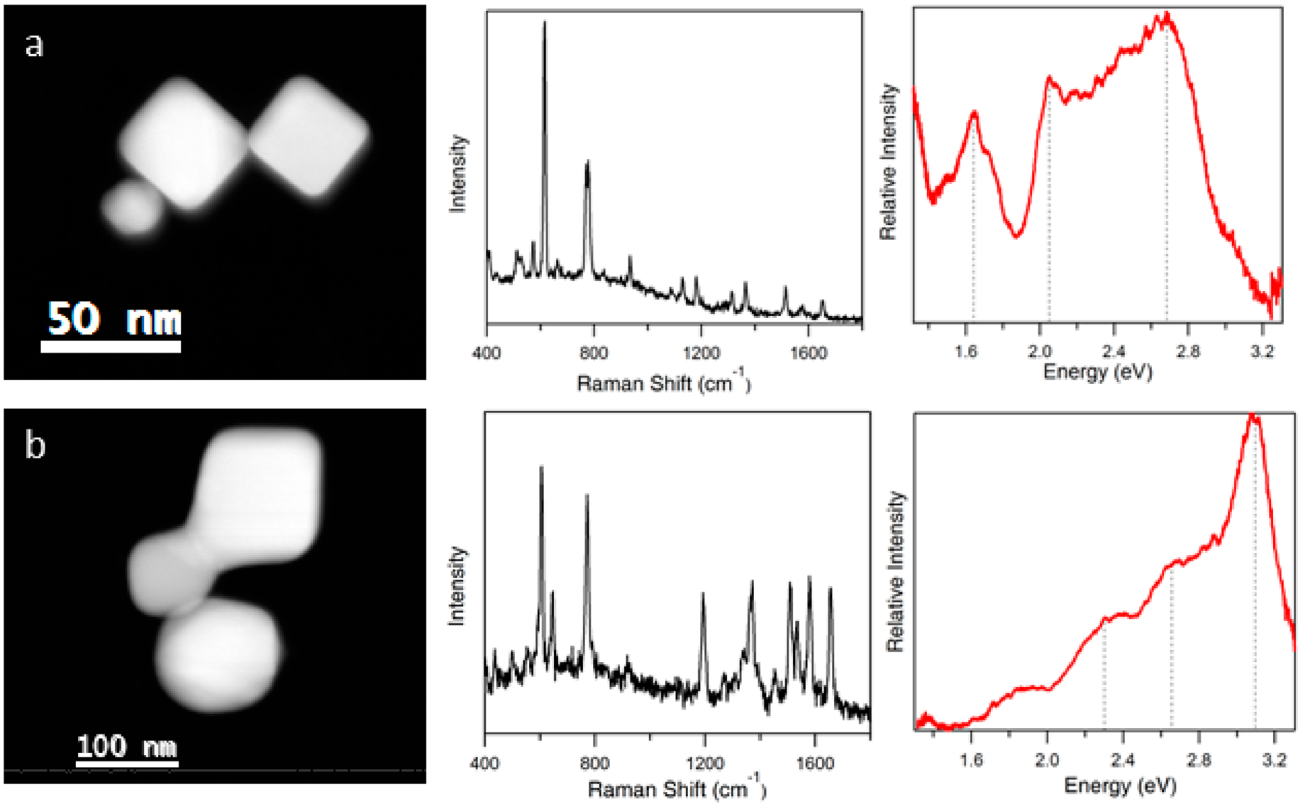

Figure 1. ADF images (left), Raman scattering (middle), and resonance-Rayleigh (right) scattering spectra of two SMSERS-active trimer structures. Single molecule character was confirmed using the isotopologue method.

junctions.[24,25] Wustholz et al.[26] demonstrated that the EFE can reach its maximum when two particles are in subnanometer proximity or have coalesced to form crevices. Studies performing high-resolution two-dimensional (2D) imaging of SMSERS hot spots measured the spatial distribution of the SMSERS centroid position and the SERS intensity,[27,28] and these studies were later expanded to include images of the active aggregates.[29] A recent theoretical investigation of the spatial, spectral, and polarization dependence of the electromagnetic SMSERS-active hot spots showed that high electromagnetic field strength can be produced at multiple *spectral* and *spatial* locations.[25] This study further demonstrated that some hot spots exist due to the collective and phase-uniform excitation of LSPRs, while others originate from interfering plasmonic excitations resulting from scattering from gaps and surfaces.

Despite the large body of evidence in favor of electromagnetic hot spots, only now have techniques emerged that can image plasmons with the spatial (<1 nm) and energy resolutions (0.1−0.3 eV) necessary to observe the elusive electromagnetic hot spots, which are thought to be essential for SMSERS. One such technique is electron-energy loss spectroscopy (EELS) in a scanning transmission electron microscopy (STEM).[30−39] The power of this technique is derived from its ability to experimentally render the photonic local density of states (LDOS). Using a Green's function approach, Garcia de Abajo and Kociak[40] concluded that "the energy loss probability is directly related to the LDOS in arbitrary systems". Numerical simulations support this conclusion, and they further emphasize the correspondence between the projection of the LDOS onto the electron trajectory and the EELS signal.[40] Hohenester, Ditlbacher, and Krenn[41] considered this same question and instead concluded that "there exists no clear-cut relation between EELS and LDOS".[41] They further examined coupled, flat metallic nanostructures and state that EELS can "be blind to the hot spots in the gap region between particles." These theoretical studies focused on structures that are quasi-planar, and it is not clear to what extent the results apply to the complex three-dimensional (3D) nanoaggregates encountered in SMSERS, where the imaging of hot spots takes on primary importance. Previous experimental studies have examined (mostly planar) coupled nanoparticle structures,[31,35,36,38,39] although none of them were known to be SMSERS-active.

Herein, we present the first STEM/EELS imaging study of plasmon modes in nanostructures *confirmed* to be SMSERS-active. Our STEM/EELS studies do *not* show an enhanced EEL in the gap regions between nanoparticles, where one would expect the electromagnetic hot spots to be located. Further, we support our experimental findings with a fully three-dimensional electrodynamics simulation of both the near-electric field enhancement (hot spot) and EELS loss probability, for the exact nanoparticle geometry obtained from the experiment. The simulations are in full agreement with the experimental results and yield insights into the specific EEL signatures associated with hot spots.

In our experiment, SMSERS-active clusters were identified using the bianalyte approach,[8,42] which relies on two isotopologues of Rhodamine 6G,[9] R6G-d_0 and R6G-d_4. Briefly, Ag nanoparticles were treated with a low concentration of the mixture of R6G-d_0 and R6G-d_4 (ca. 10^{-9} M) such that approximately one R6G molecule, either R6G-d_0 or R6G-d_4 was adsorbed per active site according to the Poisson distribution[9] (see Supporting Information (SI), Figure S1). Many SMSERS-active aggregates were analyzed with our

dx.doi.org/10.1021/jz300967q | J. Phys. Chem. Lett. 2012, 3, 2303−2309

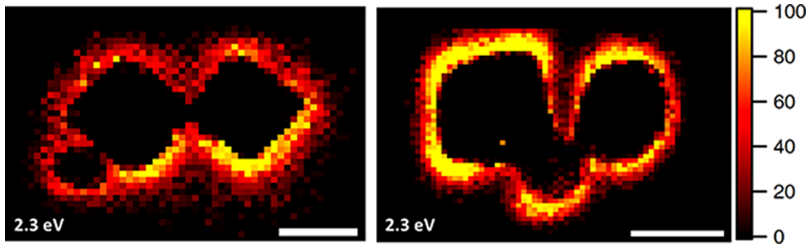

Figure 2. Spatially resolved EEL maps for a loss energy of 2.3 eV for SMSERS-active trimers. Images have been normalized to the ZLP. A complete EEL spectrum is obtained for every pixel in the region of interest (defined by the ADF in Figure 1); however, we focus on the loss energy of 2.3 eV as this corresponds to the energy of the Raman laser (532 nm, 2.3 eV) used in the SMSERS experiment. (Images for other loss features are available in the SI.) While it is assumed that the largest electromagnetic enhancement is obtained at the gap region, no localization of the EEL intensity is observed in the gaps. Scale bars are 50 nm (left) and 100 nm (right).

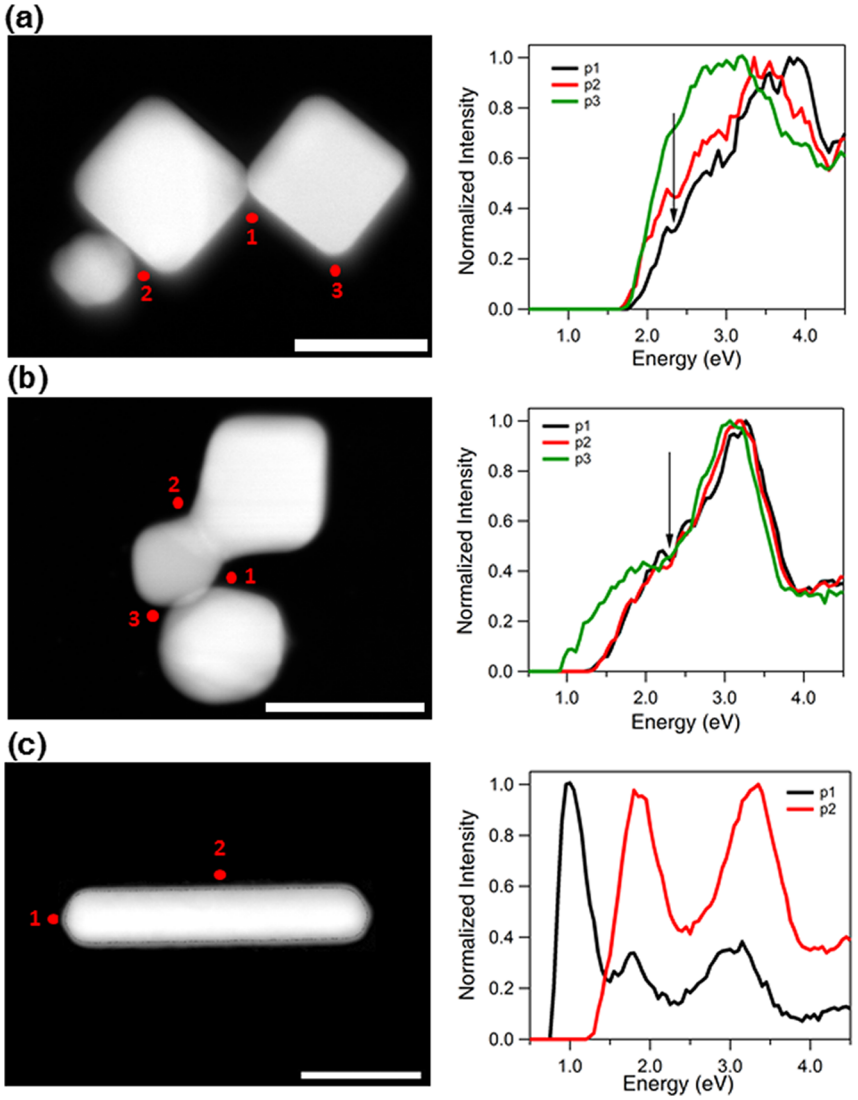

Figure 3. ADF images (left) and EEL spectra (right) for selected points around the SMSERS-active structures (a,b). For comparison, the EEL spectra and ADF images of a nanorod are adapted from ref 33. The energy of the laser line used in our experiment (532 nm ≈ 2.3 eV) is indicated with an arrow in the graphs. The spectra have been normalized so the highest point is 1. Scale bars are 50 nm (a), 100 nm (b), and 50 nm (c).

correlated STEM/EELS/optical approach to ensure a representative data set. Figure 1 presents correlated annular dark field (ADF) images and optical spectra of two representative nanostructures confirmed to be SMSERS-active. In good agreement with previous HRTEM studies,[24] our structures consist of a number of nanoparticles with varying degrees of contact. These contact regions, which we call "junctions", arise from coalesced or closely spaced structures and are thought to support electromagnetic hot spots. Figure 1 also displays the Raman spectra, without baseline or background correction, and the resonance-Rayleigh scattering measurements of the two SMSERS-active particles. As previous studies have indicated,

dx.doi.org/10.1021/jz300967q | J. Phys. Chem. Lett. 2012, 3, 2303−2309

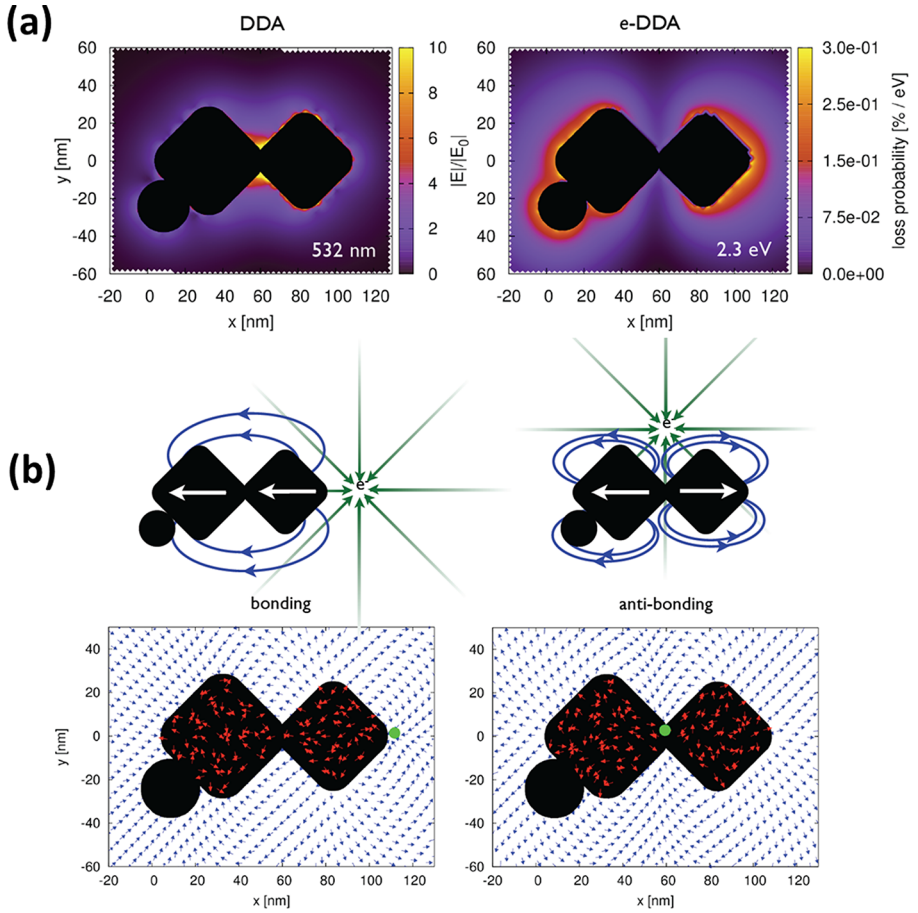

Figure 4. (a) Comparison of the calculated electric near-field magnitude obtained from plane-wave excitation (left) with the EEL probability map for a 100 keV electron beam (right) for the SMSERS-active trimer displayed in Figure 1. Simulation of the plane-wave excitation is performed via the DDA at a wavelength of 532 nm. The wave vector of the excitation field is directed along the *z*-axis and is polarized along the *x*-axis. The 2D slice displayed corresponds to the plane where the electric-field magnitude is maximized. Other polarizations, wave-vector directions, and projection planes were examined and show similar localization of the field in the junction regions. The loss-probability map, computed via the *e*-DDA, is displayed at a corresponding loss-energy of 2.3 eV. In agreement with the experiment, the EEL map does not show an intense loss probability in the junction region. (b) Induced polarization maps (2.3 eV) obtained for two different positions of the electron beam (green bullet). Placement of the electron beam in the junction leads to a net antibonding arrangement of dipoles (right), whereas placement of the electron beam on the outside right corner leads to a net bonding arrangement (left). Also shown is the induced polarization (red vectors) and resulting scattered electric field (blue vectors), both normalized to unity to aid visualization. Both panels display 2D slices taken from fully 3D simulations of the trimer. The plane of visualization was chosen to lie at the height of the centroid of the two cubes.

there is no correlation between the SERS enhancement factor and the LSPR maximum.[22,24]

When preparing SMSERS-active nanoclusters via aggregation, only a few percent of the total aggregates are found to be active.[7] This small population of active aggregates is due, in part, to the low analyte concentrations required to ensure single molecule character; however, it is additionally assumed that only "special" aggregates generate an electromagnetic hot spot on resonance with the excitation laser. In this picture, these "special" aggregates lead to the strongest SMSERS signal; although, theoretical studies[25] have cautioned that one aggregate may have multiple hot spots and that the maximum electromagnetic enhancement may be a weak function of the laser excitation energy. To examine the possibility of an electromagnetic hot spot at the energy of our resonance-Raman experiments (532 nm, 2.3 eV) we plot, in Figure 2, the spatially resolved intensity corresponding to an electron-energy-loss of 2.3 eV for the structures shown in Figure 1. We emphasize that the image obtained in Figure 2 is not dependent on the EELS data processing method. Raw energy slices of EEL (spectra after centering, normalizing to the zero loss peak (ZLP), and subtracting the ZLP), and plasmon modes extracted using the Automated eXpert Spectral Image Analysis (AXSIA) program, are similar to those presented in Figure 2 (see SI Figures S2b, S3b, S4c, S5b). These results demonstrate that there is no localization of the EEL intensity in the gaps at 2.3 eV, even at the junctions between the particles.

We have also extracted EEL spectra from the gap regions and display them in Figure 3. This allows us to probe resonances occurring at energies *different* from the excitation laser, e.g., an exceptionally bright aggregate may yield SMSERS activity, even when the laser is off resonance from the hot spot. As evident from Figure 3a,b, we do not observe any sharp resonance for either trimer at the points located between the nanoparticles. One might object that the energy resolution of the current experiment (~0.5 eV) is insufficient to resolve some of the modes (e.g., modes corresponding to the gap between the nanoparticles); therefore, for comparison, we have also included in Figure 3 EELS data for a nanorod adapted from

dx.doi.org/10.1021/jz300967q | *J. Phys. Chem. Lett.* 2012, 3, 2303−2309

our previously published work.[33] For the nanorod, we observe well-resolved (spatial and spectral) plasmon resonances.

While it is well-known that extreme near-electric-field enhancements can be obtained at locations near sharp surface protrusions or in nanogaps,[11,16,17] our EELS results do not show a clear localization of the EEL intensity at the junction of two nanoparticles. In order to examine this observation in detail, we employ a modified version of the discrete dipole approximation (DDA), called *electron-driven DDA* (*e*-DDA),[43] which imposes the electric field of a swift electron,[44,45]

$$\mathbf{E}(\mathbf{x}, \omega) = \frac{2e\omega}{v^2\epsilon\gamma} e^{i\omega z/v}\left[\frac{i}{\gamma}K_0\left(\frac{\omega b}{v\gamma}\right)\hat{\mathbf{v}} - K_1\left(\frac{\omega b}{v\gamma}\right)\hat{\mathbf{b}}\right] \quad (1)$$

rather than a plane wave upon a fully three-dimensional target located a distance $|\mathbf{x}| = (|\mathbf{b}|^2 + z^2)^{1/2}$ away from the direction of propagation, $\hat{\mathbf{v}}$. In this expression, v is the speed of the electron, chosen to propagate along the z-axis, $\gamma = [1/(1 - \epsilon(v/c)^2)^{1/2}]$, and K_0 and K_1 are modified Bessel functions. As in the DDA, the target is discretized into a finite collection of N polarizable points that are each driven by the field of the electron (eq 1) and by the electric-dipole field of all other target points. Each point is described by a linear polarizability that depends upon the complex-valued and frequency-dependent dielectric function of the bulk material.[46] When the electron beam is positioned near the target, the EEL spectra at each impact parameter $\mathbf{b}$ can be computed from the loss probability per unit frequency,[30,47]

$$P_{\mathbf{b}}(\omega) = \frac{1}{\pi\hbar}\mathrm{Im}\sum_{j=1}^{N}\mathbf{E}^*(\mathbf{x}_j, \omega)\cdot\mathbf{P}_j(\omega) \quad (2)$$

where $\mathbf{P}_j$ is the dipole moment of the jth target dipole, and $\mathbf{E}$ is the electric field of the swift electron evaluated at position j. Further details of the theoretical methods are available in the SI, and an in-depth comparison of *e*-DDA calculations with experimental STEM/EELS measurements are the subject of a companion manuscript.[43]

Figure 4(a) compares the calculated electric near-field magnitude, obtained from plane-wave excitation (DDA), and the energy-loss-probability map, obtained from a 100 keV electron beam (*e*-DDA). The calculation in both cases is performed at an energy of 2.3 eV corresponding to excitation with 532 nm light or a 2.3 eV energy loss from the electron beam.

The calculated loss-probability map (Figure 4a, right panel) compares well with the experiment (Figure 2), although small differences are observed, likely due to the complex nature of the nanoaggregates, imperfect reconstruction of the experimental ADF image to an array of dipoles, and variations in the local environment of the aggregate. Even though this structure is predicted to have an intense electromagnetic hot spot in the junction region under plane-wave excitation (Figure 4a, left panel), and is known to be SMSERS-active, a strong EEL probability in the junction region at 532 nm is *not* observed in *either* the STEM/EELS experiment or the *e*-DDA theory. We do, however, observe strong loss features at points *external* to the junctions (Figure 4).

Insight into these features can be explored by computing the polarization induced in the target at 2.3 eV for different electron-beam positions (Figure 4b). Our analysis suggests that the planar model of bonding and antibonding dipoles[41] is applicable to the more complex geometries observed in SMSERS. When the electron beam is positioned in the junction, the calculations show that a net *antibonding* arrangement of the target's polarization vectors is induced. This leads to a node of the scattered electric field in the junction and a small loss probability results. When the electron beam is positioned on the right side of the nanoaggregate, a net *bonding* arrangement of the induced polarization vectors is obtained. This underlies a capacitive electric field that is localized in the junction and is characteristic of an electromagnetic hot spot. In fact, we show in a related paper that the electron-induced junction field and the hot spot set up by plane-wave excitation are directionally identical.[43]

Both of these arrangements of the target's electronic polarization are due to the forces exerted by the polarization of the electric field of the swift electron. Interestingly, this means that the electromagnetic hot spot can indeed be excited by the electron beam, and that it is in principle possible to induce Raman scattering from the single molecule with the electron beam.

In summary, we present, for the first time, plasmon maps of SMSERS-active nanoparticles employing STEM/EELS. Although it is widely accepted that electromagnetic hot spots are responsible for SMSERS activity, and are located between the gaps of nanoparticles, we do *not* see a large EEL intensity in these regions. We have rigorously confirmed that each structure examined indeed gives rise to SMSERS before EELS imaging. Our experimental results are complemented with a fully 3D simulation that builds the electron-beam excitation directly into the DDA and utilizes shape parameters derived from the experiment. The simulations are in good agreement with the experimental results and yield insights into the specific EEL signatures associated with hot spots. In other words, the electromagnetic hot spot can be excited when the electron beam is positioned at the periphery of the nanoaggregate. With the rapid emergence of STEM/EELS as a tool for probing the plasmonic properties of nanostructures, we believe the work presented here will impact a wide range of STEM/EELS plasmon imaging experiments going forward.

METHODS

R6G-d_4 was synthesized according to the procedure described by Blackie and co-workers,[48] with NMR and mass spectrometry data of the resulting compound matching this prior report. Ag nanoparticles were treated with a low concentration of the mixture of R6G-d_0 and R6G-d_4 (ca. 10^{-9} M) such that approximately one R6G molecule, either R6G-d_0 or R6G-d_4 was adsorbed per active site according to the Poisson distribution[9] (Figure S1). Silver nanoparticles were obtained from nanoComposix and used without further purification. In our experiment, no salt was added to the SMSERS solution since previous nanoparticle studies had demonstrated the existence of sufficient aggregations, and, for the purpose of this study, simpler structures with not many overlapping nanostructures were desired. Two hundred mesh Cu grids coated with holey carbon (SPI supplies #3540C-FA) were used as TEM supports. A 3 μL aliquot of the SMSERS solution was drop-coated directly onto the TEM grid, and the solvent was allowed to evaporate. After deposition, the sample was placed on a coverslip, mounted in a custom-designed sample holder, and purged with dry nitrogen. For the Raman scattering, the sample was irradiated with 532 nm linearly polarized laser light (Spectra Physics, model J-20) at a grazing incidence with a power density of ~0.03 W/cm^2. Optical measurements were

dx.doi.org/10.1021/jz300967q | J. Phys. Chem. Lett. 2012, 3, 2303−2309

carried out on an inverted microscope (Nikon, T*i*-U) equipped with a dark field condenser (Nikon, NA = 0.95−0.80) and an ultrasteep Raman long-pass edge filter (Semrock) to block the laser Rayleigh line. Raman spectra were collected using a 100X (Nikon, 0.7 < NA < 1.4, oil immersion) objective and detected on a liquid nitrogen-cooled back-illuminated charge-coupled detector (CCD) (Princeton Instruments, PIXIS 100). Resonance-Rayleigh scattering measurements were performed on the SMSERS-active nanoparticles after removing the long-pass edge filter utilizing the unpolarized light output of a tungsten-halogen lamp. A wide-field image of the silver nanoparticles on the TEM grid was also recorded to serve as a map for subsequent characterization in the STEM. This method enabled correlated optical and STEM measurements of the exact same SMSERS-active nanostructures with an average of 15 active clusters per grid.

After identification and optical characterization of active SMSERS nanoparticles, the sample was inserted into an aberration-corrected, cold-field-emission STEM (VG Microscopes HB501UX STEM with Nion aberration corrector and Gatan Enfina EEL spectrometer). The SMSERS-active nanoparticles were found by comparing the dark-field optical map to the pattern of particles visible in the STEM at very low resolution.[49] After identification, a high-resolution ADF image and an EEL spectrum image were collected from the ZLP containing region, i.e., an EEL spectrum is recorded at each pixel over the entire region of interest. The spectrometer dispersion was set to 0.05 eV per channel with an exposure time of 0.05 s per spectrum. The pixel size/density (60 × 37 pixels for Figure 2, left and 57 × 76 pixels for Figure 2, right, with a spatial resolution of ∼3 nm per pixel) was chosen to give a total acquisition time of around 11 min for a single spectrum image. Shorter acquisition times were used to avoid accumulation of contaminations caused by the electron beam. The energy resolution, determined by the full-width-half-maximum of the ZLP, was ∼0.5−0.55 eV. The STEM/EELS data were analyzed using three different approaches: in the first approach, the raw EELS data were examined after centering the ZLP of each spectrum at 0 eV, normalizing to the ZLP, and subtracting the ZLP, leaving only the inelastic contributions to the spectrum image. In the second approach, for a particular pixel of interest, the complete EEL spectra, after centering and subtracting the ZLP, were background subtracted and plotted for different probe positions on the entire structure. In a third and final approach, multivariate statistical analysis employing the AXSIA program,[50,51] was applied to the data to extract statistically significant component spectra and maps; details of this analysis have been discussed in our previously published work.[33] The data analysis using AXSIA is presented in the SI. Our experimental measurements are also supported by electrodynamics simulations based on the DDA,[52,53] and the details are presented in the SI.

■ ASSOCIATED CONTENT

Supporting Information

Simulation methods and additional figures (S1−S5). This material is available free of charge via the Internet at http://pubs.acs.org

■ AUTHOR INFORMATION

Corresponding Author

*E-mail: masiello@u.washington.edu (D.J.M); beth.guiton@uky.edu (B.S.G); jcamden@utk.edu (J.P.C.).

Author Contributions

#These authors contributed equally to this work.

Notes

The authors declare no competing financial interest.

■ ACKNOWLEDGMENTS

This research was supported by the Eugene P. Wigner Fellowship program of the Oak Ridge National Laboratory and University of Kentucky (B.S.G.), University of Tennessee (UT) Office of Research, College of Arts and Sciences, and Department of Chemistry, the UT/ORNL Joint Institute for Advanced Materials, and the U.S. Department of Energy, Office of Basic Energy Sciences, under Award Number DE-SC0004792 (V.I., N.M.K., J.P.C.); the Office of Basic Energy Sciences, Materials Sciences and Engineering Division, U.S. Department of Energy (S.J.P.); the National Science Foundation under Awards CHE-0954297 and DMR-0906752 (M.D.B., M.M.R.); the University of Washington College of Arts and Sciences and Department of Chemistry (N.W.B., A.V., D.J.M.). N.M.K. and V.I. also thank Dr. Andrew R. Lupini for assistance with the EELS data analysis.

■ REFERENCES

(1) Fleischman, M.; Hendra, P. J.; McQuilla, A. J. Raman-Spectra of Pyridine Adsorbed at a Silver Electrode. *Chem. Phys. Lett.* **1974**, *26*, 163−166.

(2) Albrecht, M. G.; Creighton, J. A. Anomalously Intense Raman-Spectra of Pyridine at a Silver Electrode. *J. Am. Chem. Soc.* **1977**, *99*, 5215−5217.

(3) Jeanmaire, D. L.; Vanduyne, R. P. Surface Raman Spectroelectrochemistry 0.1. Heterocyclic, Aromatic, and Aliphatic-Amines Adsorbed on Anodized Silver Electrode. *J. Electroanal. Chem.* **1977**, *84*, 1−20.

(4) Maier, S. A.; Brongersma, M. L.; Kik, P. G.; Meltzer, S.; Requicha, A. A. G.; Atwater, H. A. Plasmonics - A Route to Nanoscale Optical Devices. *Adv. Mater.* **2001**, *13*, 1501−1505.

(5) Moskovits, M. Surface-Ehanced Spectroscopy. *Rev. Mod. Phys.* **1985**, *57*, 783−826.

(6) Kneipp, K.; Wang, Y.; Kneipp, H.; Perelman, L. T.; Itzkan, I.; Dasari, R.; Feld, M. S. Single Molecule Detection Using Surface-Enhanced Raman Scattering (SERS). *Phys. Rev. Lett.* **1997**, *78*, 1667−1670.

(7) Nie, S. M.; Emery, S. R. Probing Single Molecules and Single Nanoparticles by Surface-Enhanced Raman Scattering. *Science* **1997**, *275*, 1102−1106.

(8) Le Ru, E. C.; Meyer, M.; Etchegoin, P. G. Proof of Single-Molecule Sensitivity in Surface Enhanced Raman Scattering (SERS) by Means of a Two-Analyte Technique. *J. Phys. Chem. B* **2006**, *110*, 1944−1948.

(9) Dieringer, J. A.; Lettan, R. B.; Scheidt, K. A.; Van Duyne, R. P. A Frequency Domain Existence Proof of Single-Molecule Surface-Enhanced Raman Spectroscopy. *J. Am. Chem. Soc.* **2007**, *129*, 16249−16256.

(10) Etchegoin, P. G.; Le Ru, E. C. A Perspective on Single Molecule Sers: Current Status and Future Challenges. *Phys. Chem. Chem. Phys.* **2008**, *10*, 6079−6089.

(11) Xu, H. X.; Aizpurua, J.; Kall, M.; Apell, P. Electromagnetic Contributions to Single-Molecule Sensitivity in Surface-Enhanced Raman Scattering. *Phys. Rev. E* **2000**, *62*, 4318−4324.

(12) Jensen, T. R.; Malinsky, M. D.; Haynes, C. L.; Van Duyne, R. P. Nanosphere Lithography: Tunable Localized Surface Plasmon Resonance Spectra of Silver Nanoparticles. *J. Phys. Chem. B* **2000**, *104*, 10549−10556.

(13) Petryayeva, E.; Krull, U. J. Localized Surface Plasmon Resonance: Nanostructures, Bioassays and Biosensing − A Review. *Anal. Chim. Acta* **2011**, *706*, 8−24.

(14) Fan, M.; Andrade, G. F. S.; Brolo, A. G. A Review on the Fabrication of Substrates for Surface Enhanced Raman Spectroscopy and Their Applications in Analytical Chemistry. *Anal. Chim. Acta* **2011**, *693*, 7−25.
(15) Schatz, G. C.; Duyne, R. P. V. Electromagnetic Mechanism of Surface-Enhanced Spectroscopy. In *Handbook of Vibrational Spectroscopy*; Chalmers, J. M.; Griffiths, P. R., Eds.; John Wiley & Sons Ltd: New York, 2002.
(16) Johansson, P.; Xu, H. X.; Kall, M. Surface-Enhanced Raman Scattering and Fluorescence near Metal Nanoparticles. *Phys. Rev. B* **2005**, *72*, 035427.
(17) Le Ru, E. C.; Etchegoin, P. G.; Meyer, M. Enhancement Factor Distribution around a Single Surface-Enhanced Raman Scattering Hot Spot and Its Relation to Single Molecule Detection. *J. Chem. Phys.* **2006**, *125*, 204701.
(18) Marinica, D. C.; Kazansky, A. K.; Nordlander, P.; Aizpurua, J.; Borisov, A. G. Quantum Plasmonics: Nonlinear Effects in the Field Enhancement of a Plasmonic Nanoparticle Dimer. *Nano Lett.* **2012**, *12*, 1333−9.
(19) Le Ru, E. C.; Blackie, E.; Meyer, M.; Etchegoin, P. G. Surface Enhanced Raman Scattering Enhancement Factors: A Comprehensive Study. *J. Phys. Chem. C* **2007**, *111*, 13794−13803.
(20) Gersten, J.; Nitzan, A. Electromagnetic Theory of Enhanced Raman-Scattering by Molecules Adsorbed on Rough Surfaces. *J. Chem. Phys.* **1980**, *73*, 3023−3037.
(21) Metiu, H.; Das, P. The Electromagnetic Theory of Surface Enhanced Spectroscopy. *Annu. Rev. Phys. Chem.* **1984**, *35*, 507−536.
(22) Michaels, A. M.; Jiang, J.; Brus, L. Ag Nanocrystal Junctions as the Site for Surface-Enhanced Raman Scattering of Single Rhodamine 6G Molecules. *J. Phys. Chem. B* **2000**, *104*, 11965−11971.
(23) Michaels, A. M.; Nirmal, M.; Brus, L. E. Surface Enhanced Raman Spectroscopy of Individual Rhodamine 6G Molecules on Large Ag Nanocrystals. *J. Am. Chem. Soc.* **1999**, *121*, 9932−9939.
(24) Camden, J. P.; Dieringer, J. A.; Wang, Y.; Masiello, D. J.; Marks, L. D.; Schatz, G. C.; Van Duyne, R. P. Probing the Structure of Single-Molecule Surface-Enhanced Raman Scattering Hot Spots. *J. Am. Chem. Soc.* **2008**, *130*, 12616−12617.
(25) Litz, J. P.; Camden, J. P.; Masiello, D. J. Spatial, Spectral, and Coherence Mapping of Single-Molecule Sers Active Hot Spots Via the Discrete-Dipole Approximation. *J. Phys. Chem. Lett.* **2011**, *2*, 1695−1700.
(26) Wustholz, K. L.; Henry, A.-I.; McMahon, J. M.; Freeman, R. G.; Valley, N.; Piotti, M. E.; Natan, M. J.; Schatz, G. C.; Van Duyne, R. P. Structure-Activity Relationships in Gold Nanoparticle Dimers and Trimers for Surface-Enhanced Raman Spectroscopy. *J. Am. Chem. Soc.* **2010**, *132*, 10903−10910.
(27) Cang, H.; Labno, A.; Lu, C.; Yin, X.; Liu, M.; Gladden, C.; Liu, Y.; Zhang, X. Probing the Electromagnetic Field of a 15-Nanometre Hotspot by Single Molecule Imaging. *Nature* **2011**, *469*, 385−388.
(28) Stranahan, S. M.; Willets, K. A. Super-Resolution Optical Imaging of Single-Molecule SERS Hot Spots. *Nano Lett.* **2010**, *10*, 3777−3784.
(29) Willets, K. A.; Stranahan, S. M.; Weber, M. L. Shedding Light on Surface-Enhanced Raman Scattering Hot Spots through Single-Molecule Super-Resolution Imaging. *J. Phys. Chem. Lett.* **2012**, *3*, 1286−1294.
(30) Garcia de Abajo, F. J. Optical Excitations in Electron Microscopy. *Rev. Mod. Phys.* **2010**, *82*, 209−275.
(31) Bosman, M.; Keast, V. J.; Watanabe, M.; Maaroof, A. I.; Cortie, M. B. Mapping Surface Plasmons at the Nanometre Scale with an Electron Beam. *Nanotechnology* **2007**, *18*, 165505.
(32) Nelayah, J.; Kociak, M.; Stephan, O.; Garcia de Abajo, F. J.; Tence, M.; Henrard, L.; Taverna, D.; Pastoriza-Santos, I.; Liz-Marzan, L. M.; Colliex, C. Mapping Surface Plasmons on a Single Metallic Nanoparticle. *Nat. Phys.* **2007**, *3*, 348−353.
(33) Guiton, B. S.; Iberi, V.; Li, S.; Leonard, D. N.; Parish, C. M.; Kotula, P. G.; Varela, M.; Schatz, G. C.; Pennycook, S. J.; Camden, J. P. Correlated Optical Measurements and Plasmon Mapping of Silver Nanorods. *Nano Lett.* **2011**, *11*, 3482−3488.
(34) Nicoletti, O.; Wubs, M.; Mortensen, N. A.; Sigle, W.; van Aken, P. A.; Midgley, P. A. Surface Plasmon Modes of a Single Silver Nanorod: An Electron Energy Loss Study. *Opt. Express* **2011**, *19*, 15371−15379.
(35) Chu, M. W.; Myroshnychenko, V.; Chen, C. H.; Deng, J. P.; Mou, C. Y.; de Abajo, F. J. G. Probing Bright and Dark Surface-Plasmon Modes in Individual and Coupled Noble Metal Nanoparticles Using an Electron Beam. *Nano Lett.* **2009**, *9*, 399−404.
(36) Koh, A. L.; Fernandez-Dominguez, A. I.; McComb, D. W.; Maier, S. A.; Yang, J. K. W. High-Resolution Mapping of Electron-Beam-Excited Plasmon Modes in Lithographically Defined Gold Nanostructures. *Nano Lett.* **2011**, *11*, 1323−1330.
(37) Scholl, J. A.; Koh, A. L.; Dionne, J. A. Quantum Plasmon Resonances of Individual Metallic Nanoparticles. *Nature* **2012**, *483*, 421−427.
(38) Duan, H.; Fernandez-Dominguez, A. I.; Bosman, M.; Maier, S. A.; Yang, J. K. W. Nanoplasmonics: Classical Down to the Nanometer Scale. *Nano Lett.* **2012**, *12*, 1683−1689.
(39) Koh, A. L.; Bao, K.; Khan, I.; Smith, W. E.; Kothleitner, G.; Nordlander, P.; Maier, S. A.; McComb, D. W. Electron Energy-Loss Spectroscopy (EELS) of Surface Plasmons in Single Silver Nanoparticles and Dimers: Influence of Beam Damage and Mapping of Dark Modes. *ACS Nano* **2009**, *3*, 3015−3022.
(40) Garcia de Abajo, F. J.; Kociak, M. Probing the Photonic Local Density of States with Electron Energy Loss Spectroscopy. *Phys. Rev. Lett.* **2008**, *100*, 106804.
(41) Hohenester, U.; Ditlbacher, H.; Krenn, J. R. Electron-Energy-Loss Spectra of Plasmonic Nanoparticles. *Phys. Rev. Lett.* **2009**, *103*, 106801.
(42) Etchegoin, P. G.; Meyer, M.; Blackie, E.; Le Ru, E. C. Statistics of Single-Molecule Surface Enhanced Raman Scattering Signals: Fluctuation Analysis with Multiple Analyte Techniques. *Anal. Chem.* **2007**, *79*, 8411−8415.
(43) Bigelow, N. W.; Vaschillo, A.; Iberi, V.; Camden, J. P.; Masiello, D. J. Characterization of the Electron- and Photon-Driven Plasmonic Excitations of Metal Nanorods. *ACS Nano* **2012**, DOI: 10.1021/nn302980u.
(44) Ritchie, R. H.; Howie, A. Electron-Excitation and Optical-Potential in Electron-Microscopy. *Philos. Mag.* **1977**, *36*, 463−481.
(45) Rose, H. Image-Formation by Inelastically Scattered Electrons in Electron-Microscopy. *Optik* **1976**, *45*, 139−158.
(46) Lynch, D. W.; Hunter, W. R. In *Handbook of Optical Constant of Solids*; Palik, E. D., Ed.; Academic Press: New York, 1998.
(47) Muller, D. A.; Silcox, J. Delocalization in Inelastic-Scattering. *Ultramicroscopy* **1995**, *59*, 195−213.
(48) Blackie, E.; Le Ru, E. C.; Meyer, M.; Timmer, M.; Burkett, B.; Northcote, P.; Etchegoin, P. G. Bi-analyte SERS with Isotopically Edited Dyes. *Phys. Chem. Chem. Phys.* **2008**, *10*, 4147−4153.
(49) Wang, Y.; Eswaramoorthy, S. K.; Sherry, L. J.; Dieringer, J. A.; Camden, J. P.; Schatz, G. C.; Van Duyne, R. P.; Marks, L. D. A Method to Correlate Optical Properties and Structures of Metallic Nanoparticles. *Ultramicroscopy* **2009**, *109*, 1110−1113.
(50) Keenan, M. R. Exploiting Spatial-Domain Simplicity in Spectral Image Analysis. *Surf. Interface Anal.* **2009**, *41*, 79−87.
(51) Kotula, P. G.; Keenan, M. R.; Michael, J. R. Automated Analysis of SEM X-Ray Spectral Images: A Powerful New Microanalysis Tool. *Microsc. Microanal.* **2003**, *9*, 1−17.
(52) Draine, B. T.; Flatau, P. J. Discrete-Dipole Approximation for Scattering Calculations. *J. Opt. Soc. Am. A* **1994**, *11*, 1491−1499.
(53) Draine, B. T.; Flatau, P. J. Discrete-Dipole Approximation for Periodic Targets: Theory and Tests. *J. Opt. Soc. Am. A* **2008**, *25*, 2693−2703.